International Journal for Housing Science and Its Applications
Publish August 4, 2025. Volume 46, Issue 3 Pages 2666-2676

https://doi.org/10.70517/ijhsa463224

Extraction of time-varying laws of electrical characteristics of converter valves and health monitoring based on modal analysis and multi-source data fusion

Zhen Wang[1,*], Linhao Xu[1] and Ao Feng[2]
[1] China Southern Power Grid Digital Grid Research Institute Co., Ltd., Guangzhou, Guangdong, 510555, China
[2] Wuhan University, Wuhan, Hubei, 430072, China
Corresponding authors: (e-mail: zlxn0011@outlook.com).

Abstract As the core equipment of high-voltage direct current (HVDC) transmission system, the health status of the converter valve directly affects the stability of power grid operation. In this paper, we propose a fusion of modal analysis and multi-source data-driven method for extracting the time-varying laws of electrical features and health monitoring of the converter valve. The multidimensional vibration feature map is constructed, and the multi-scale features of the vibration signal are extracted by combining the time-domain trajectory image, Markov variation field and wavelet packet transform. The short-circuit fault characteristics and protection principle of the converter valve are analyzed, and a valve state discrimination model based on current timing characteristics is established. The effectiveness of the method is verified through simulation and engineering experiments, and the proposed method can realize the state discrimination of converter valve fault characteristics. Considering all 405 power modules of the whole bridge arm, the error of capacitance capacity estimation based on field data is within 1%, and the accuracy of fault detection for short circuit on AC side of converter valve, short circuit on converter valve and short circuit on DC side of converter valve reaches 99.88%, 99.86% and 99.91%, respectively.

Index Terms converter valve, fault characterization, timing characteristics, valve state discrimination, health monitoring

I. Introduction

The converter valve is a high-tech product integrating high voltage, power electronics, automatic control, microelectronics, optoelectronic technology, etc. Its main roles are long-distance high-power high-voltage direct current transmission and cross-region grid interconnection, and its value accounts for about 22% of the total price of its complete set of direct current equipment [1]-[4].

As the core equipment of high-voltage DC transmission system, its structural design directly affects the power conversion efficiency and system stability [5], [6]. The whole set of devices consists of four major parts, namely, valve-based electronic equipment, thyristor stage, damping circuit, and cooling system, and each subsystem has a precise technical synergy relationship [7], [8]. Among them, the thyristor is the core component of the converter valve, which determines the current throughput capacity of the converter valve (at present, China has developed a 6-inch thyristor with a rated current throughput capacity of 4,000 amperes), and the desired system voltage can be obtained by connecting multiple thyristor elements in series [9]-[11]. The triggering methods of thyristors are categorized into electrical and optical triggering, of which ABB and Siemens and AIFF are representatives, respectively [12]. And the valve-based electronic device serves as the control center, which contains the real-time monitoring module and the trigger pulse generator [13], [14]. The monitoring module adopts fiber-optic temperature sensors to collect data from more than 2,000 measurement points in real time, and the trigger pulse generator generates accurate 0.1 μs-level trigger signals through an optoelectronic conversion device [15], [16]. However, the converter valve will be affected by various factors in the process of operation, and its performance and safety are not guaranteed. Therefore, the time-varying law extraction and health monitoring of the electrical characteristics of the converter valve are of great significance for the converter valve to be able to enhance the reliability of the equipment, the safety of the system, and the economy of operation and maintenance.

In this paper, the time domain feature mapping of the main circulation pump is constructed based on the time domain feature extraction method of vibration trajectory image and pseudo-color coding. The frequency domain and time-frequency domain feature maps of the main circulation pump are constructed by integrating Markov variation field and wavelet packet transform. Analyze the electromagnetic transient characteristics of short-circuit faults in the

AC side, DC side and valve body of the converter valve, and establish the dual threshold criterion and bypass loop state correction mechanism for valve short-circuit protection. Using the timing characteristics of AC and DC currents, the on/off state of each valve is predicted. The accuracy and practicability of the proposed method in fault location and valve current calculation are compared and analyzed by MATLAB simulation and an engineering measurement data.

II. The design of time-varying law extraction and state discrimination method for converter valve electrical features

II. A. Multi-dimensional vibration feature mapping construction

The vibration signals of the main circulation pump of the converter valve change rapidly in amplitude and have high signal complexity, which are typical non-stationary sequences, so the fault characteristics are reflected in multi-dimensional levels such as the time-frequency domain. In addition, because the vibration signal maintains a strong dependence on time, the feature maps used for fault diagnosis should retain the temporal and spatial feature information in the original vibration signal as much as possible. To solve the above problems, this paper combines vibration trajectory images and color coding methods to extract the time domain features of vibration signals. Combining the Markov variation field and wavelet packet transform, the low and high frequency domain information in the vibration signal is extracted respectively, which is used to characterize the frequency domain and time-frequency domain features.

II. A. 1) Time domain feature mapping construction

(1) Multi-dimensional vibration trajectory image

Due to the changes in the operating conditions and fault types of the main circulation pump, periodic shock components may occur in different parts of the equipment. In order to obtain complete fault characteristic information, the vibration signals are measured from three directions: horizontal radial, vertical radial and axial. Since the vibration signals are typical time series signals and are orthogonal in space, they can reflect the vibration of each part and each direction of the main circulating pump under the fault condition.

By correlating the vibration signals in each direction and transforming them into vibration trajectory images, a feature map containing time-domain fault information of the equipment is constructed. Take the vertical radial vibration signal $X=[x_1,x_2,\cdots,x_n]$ as an example, where x_i is the i th element in the vertical radial vibration signal X, and n is the number of signal sampling points. The basic steps of vibration trajectory image construction are as follows.

a) Segmented aggregation approximation. Due to the strong fluctuation of high-frequency vibration signals, the segmented aggregation approximation method (PAA) is used to find the average value of each m points to aggregate the vibration signal sequence, so as to realize the smoothing of vibration signals. Its calculation formula is:

$$\hat{x}_i=\frac{x_{m(i-1)+1}+x_{m(i-1)+2}+\cdots+x_{mi}}{m} \tag{1}$$

where: $\hat{x}_i$ represents the i rd element of the vibration signal $\hat{X}$ after PAA; x_{mi} represents the mi th element of the original vibration signal X, and the value of subscript i ranges from 1 to $\lfloor n/m \rfloor$, $\lfloor n/m \rfloor$ is the length of the vibration signal sequence after PAA, and a good signal smoothing effect can be achieved by selecting $m=2$.

b) Signal normalization. In order to reflect the complete fault information in the vibration signals, it is necessary to intercept the sequence of vibration signals with a length of more than one complete vibration cycle T. In order to facilitate the further setting of the resolution of the vibration trajectory image, the vertical radial vibration signal $\hat{X}$ after PPA is normalized. Its calculation formula is:

$$\hat{x}_i'=\frac{\hat{x}_i-\hat{x}_{\min}}{\hat{x}_{\max}-\hat{x}_{\min}} \tag{2}$$

where: $\hat{x}_{\max}$ and $\hat{x}_{\min}$ are the maximum and minimum values, respectively, in the sequence of vibration signals $\hat{X}$ after PAA; and $\hat{x}_i'$ is the i th element of the sequence of normalized vibration signals $\hat{X}'$ of the i th element.

c) Set the resolution. In this paper, the element $\hat{x}_i'$ in the normalized vibration signal sequence $\hat{X}'$ is rounded

down to get the integer vibration sequence $\hat{X}''$ and used to construct the vibration trajectory image. And the size of image resolution r determines the structural complexity and fitting speed of the fault diagnosis model. Its calculation formula is:

$$\hat{x}_i'' = f_{floor}\left(r \times \hat{x}_i'\right) \tag{3}$$

where: $f_{floor}(\cdot)$ denotes the downward rounding function; $\hat{x}_i''$ is the i th element in the integer vibrational sequence $\hat{X}''$; and r is the resolution, which takes the value of 250.

d) Construct the vibration trajectory image. Perform the operations of the previous steps 1) - 3) for the horizontal radial vibration signal $Y=[y_1, y_2, \cdots, y_n]$ to obtain a new integer vibration sequence $\hat{Y}''=[y_1'', y_2'', \cdots, y_n'']$. Create a set of zero matrices V of size $r \times r$. Traverse the vertical radial vibration sequence $\hat{X}''$ and the horizontal radial vibration sequence $\hat{Y}''$ over a complete vibration period, and sequentially assign the corresponding element of the zero matrix to a value of 1. The formula is:

$$V=\begin{bmatrix} 0 & \cdots & 0 & 0 \\ \vdots & & \vdots & \vdots \\ 0 & \cdots & v_{kl} & 0 \\ 0 & \cdots & 0 & 0 \end{bmatrix}\left(v_{kl}=0\right) \tag{4}$$

$$v_{kl}=1\left(k=\hat{x}_{i''}, l=\hat{y}_{i''}, i=1, \cdots, \lfloor n/m \rfloor\right) \tag{5}$$

where V is the multidimensional vibrating trajectory image; y_i and $\hat{y}_i''$ are the i th element in the sequences Y and $\hat{Y}''$, respectively; and v_{kl} is the the k th row and l th column element of the matrix V, whose value is initialized to 0 and updated according to Eq. (5).

e) Multi-dimensional vibration trajectory image generation. The vibration trajectory images based on horizontal radial and axial directions, as well as axial and vertical radial directions can be created simultaneously using the above method to realize the vibration feature extraction in different directions of the main circulation pump.

(2) Pseudo-color coding processing

During the process of creating vibration trajectory images of vibration signals, information loss is inevitably caused. It is necessary to add additional feature quantities in the vibration trajectory image for expanding the fault characteristic information of the map. In this paper, the vibration signals in three directions are used to construct the Red matrix channel, Green matrix channel and Blue matrix channel in the RGB color space, respectively. Each of these matrix channels has the same pixel value as the vibration trace image, and the vibration trace image is processed by pseudo-color coding through data mapping. Taking the construction of Red matrix channel by horizontal radial vibration signal as an example, the process of color coding is as follows.

a) Construct color coding vectors. The amplitude information in the time domain of the signal is converted into a coding vector suitable for image recognition. Take the horizontal radial-based vibration signal $\hat{Y}''$ as an example, construct the color coding vector c.

$$U_i = f_{where}\left(\hat{y}_j''=i\right)\left(j=1,2,\cdots,\lfloor n/m \rfloor\right) \tag{6}$$

$$c_i = \sum_{j \in U_i} \hat{y}_j \left(i=1,2,\cdots,r\right) \tag{7}$$

where $\hat{y}_{j''}$ is the j th element of the integer vibrational sequence $\hat{Y}''$; U_i denotes the set of all subscripts j that make the expression $\hat{y}_{j''}=i$ hold; $f_{where}(\cdot)$ is the get subscript function; c_i denotes the i th element of the color coding vector c.

b) Construct the color coding matrix. The obtained color vectors are vertically stacked r columns to form a color-coded matrix C of size $r \times r$.

$$C=\begin{bmatrix} c_1 & c_1 & \cdots & c_1 \\ c_2 & c_2 & \cdots & c_2 \\ \vdots & \vdots & & \vdots \\ c_r & c_r & \cdots & c_r \end{bmatrix}_{r\times r} \tag{8}$$

c) Element mapping. The color matrix is elementally mapped to the vibration trajectory image to achieve the color coding of the vibration trajectory image. Its calculation formula is:

$$V'=V \square C \tag{9}$$

where: V' is the color-coded multidimensional vibrational trajectory image; $\square$ denotes matrix multiplication by elements.

II. A. 2) Frequency domain feature mapping construction

The main circulation pump, as the core rotating equipment, fails to introduce a periodic shock component in the vibration signal. At the same time, the equipment is affected by the inherent vibration frequency and environmental noise, and the vibration signal shows broadband vibration characteristics including periodicity and non-periodicity.

In the early stage of fault development, the vibration characteristics are mainly manifested as periodic shock signals dominated by fundamental and octave frequency components. According to the sampling theorem, the effective measurement frequency of the vibration sensor is within 5000 Hz, and the main frequency of the vibration of the main pump is concentrated in 20~200 Hz. Based on the Markov variation field, the frequency domain feature map is constructed to amplify the spectral characteristics of the vibration signal in the low-frequency band. The specific steps of constructing the frequency domain feature map are as follows.

(1) Low-frequency refinement analysis. In order to refine the low-frequency part of the signal and prevent frequency aliasing, an eighth-order Butterworth low-pass filter with a cutoff frequency of 500 Hz is used to filter out the high-frequency noise in the vibration signal. The filtered low-frequency signal is resampled and the Fourier transform is used to obtain the refined low-frequency sequence.

(2) Constructing the transfer matrix. In the process of constructing the frequency domain feature mapping, the temporal correlation of the original sequence needs to be maintained. Based on the transfer probability characterizing the temporal information of the original one-dimensional data, the Markov variation field can convert the refined frequency sequence into a frequency feature map. Taking the refined frequency sequence $F=\left[f_1,f_2,\cdots,f_n\right]$ of the axial vibration signal under the angular misalignment fault state as an example, the data in the sequence are mapped to the quartiles q_t by dividing F into Q-quartile regions (where the t takes values ranging from 1 to Q). Based on the leapfrog relationship between quartiles, the transfer matrix W is constructed along the time axis in the manner of a first-order Markov chain, and the expression is shown in Equation (10).

$$W=\begin{bmatrix} \omega_{11|P(f_t\in q_1|f_{t-1}\in q_1)} & \cdots & \omega_{1Q|P(f_t\in q_1|f_{t-1}\in q_Q)} \\ \omega_{21|P(f_t\in q_2|f_{t-1}\in q_1)} & \cdots & \omega_{2Q|P(f_t\in q_2|f_{t-1}\in q_Q)} \\ \vdots & & \vdots \\ \omega_{Q1|P(f_t\in q_Q|f_{t-1}\in q_1)} & \cdots & \omega_{QQ|P(f_t\in q_Q|f_{t-1}\in q_Q)} \end{bmatrix} \tag{10}$$

where: $\omega_{ij|P(f_t\in q_i|f_{t-1}\in q_j)}$ is the element of the i th row and j th column of the transfer matrix W, which is numerically equal to the probability that quartile q_i is located after quartile q_j, $P\left(f_t\in q_i \mid f_{t-1}\in q_j\right)$; f_t and f_{t-1} are the t and $t-1$ elements of the refined frequency sequence F, respectively.

(3) Construction of Markovian transfer field. To overcome the problem of weak dependence of the transfer matrix on the time step, the signal timing information is preserved by extending the transfer matrix W into a Markov variation field M. The formula is shown in Eq. (11).

$$M=\begin{bmatrix} m_{ij|f_1\in q_i,f_1\in q_j} & \cdots & m_{ij|f_1\in q_i,f_n\in q_j} \\ m_{ij|f_2\in q_i,f_1\in q_j} & \cdots & m_{ij|f_2\in q_i,f_n\in q_j} \\ \vdots & & \vdots \\ m_{ij|f_n\in q_i,f_1\in q_j} & \cdots & m_{ij|f_n\in q_i,f_n\in q_j} \end{bmatrix} \tag{11}$$

where $m_{ij|f_1 \in q_i, f_1 \in q_j}$ denotes the transfer probability of quartile q_i to quartile q_j, i.e., $m_{ij|f_1 \in q_i, f_1 \in q_j} = P(q_i \to q_j)$, where the values of i and j are in the range of 1 to Q.

The Markov variation field M transforms the values in the frequency sequence into state values, and by calculating the transformation probability of the time series, it can represent the relationship between data at any two time points in the time series data, which captures the variation information of the refined frequency sequence in the form of feature mapping.

II. A. 3) Time-frequency domain feature mapping construction

With the development of the main circulating pump failure stage, minor failures may cause the inherent frequency vibration of the equipment, and the failure frequency ranges from 500 to 2000 Hz. The high-frequency components of the vibration signal also contain a large amount of detailed information. The wavelet packet transform realizes equal bandwidth fine filtering for the high frequency band signals not decomposed in the wavelet transform. Therefore, based on the wavelet packet decomposition, it can realize time-frequency domain feature extraction, especially for the high-frequency band with higher time-frequency resolution.

In this paper, the “Morlet” wavelet is used as the wavelet basis function, and the “Morlet” wavelet basis function consists of a complex trigonometric function multiplied by an exponential decay function, and the function is defined as shown in equation (12).

$$\psi(x) = \beta e^{-\frac{x^2}{2}} \cos(i w_0 x) \tag{12}$$

where: $\psi(x)$ is the wavelet basis function; x is the independent variable; β is the amplitude; i is the imaginary unit; w_0 is the center frequency of the decay function.

The maximum number of decomposition layers is chosen to be 3, thus obtaining 8 vibration signal components. Since the components show the variation of the signal in different frequency bands with time, they can be used as the characteristic expression of the signal in the time-frequency domain. After sorting the wavelet packet nodes obtained from the decomposition based on the frequency bands, the vertical arrangement is used to construct the time-frequency domain feature maps.

II. B.Failure point analysis of converter valve

At present, each pole of UHV DC converter station is configured with high and low end series structure of double 12 pulsating converter, and the typical operation mode of DC includes double large pole earth return line, single pole earth return line and single pole metal return line. The fault characteristics of the converter valve are basically the same in the typical operation mode. The real-time digital system simulation (RTDS) analysis is carried out in the typical operation mode of bipolar four-valve earth return as an example. The short-circuit faults in the converter valve area mainly include short-circuit in the AC side of the converter valve, short-circuit in the converter valve, short-circuit in the DC side of the converter valve, and the typical fault points in the valve area on the rectifier side are shown in Figure 1. In Fig. 1, V_{11}, V_{21}, V_{31}, V_{41}, V_{51}, V_{61} indicate Y-bridge six pulsating converter valves, and V_{12}, V_{22}, V_{32}, V_{42}, V_{52}, V_{62} indicate D bridge six pulsating commutator valve.

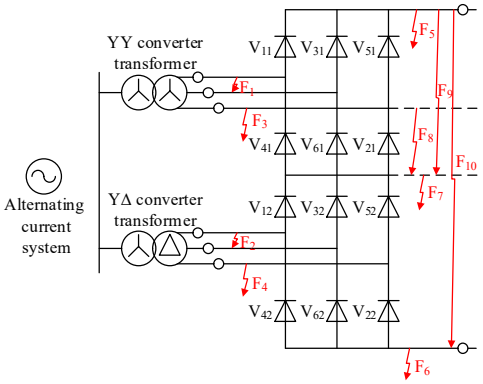

Figure 1: Typical fault point of short circuit of rectifier side valve

The short circuit on the AC side of the converter valve mainly includes the short circuit between phases on the

valve side of the converter transformer F_1, F_2 and the single-phase grounding short circuit on the valve side of the converter transformer F_3, F_4. The short circuit of DC side of converter valve mainly includes short circuit of high voltage side grounding of converter valve F_5, short circuit of low voltage side grounding of converter valve F_6, and grounding of midpoint of converter valve F_7. Converter valve short circuit mainly includes single valve short circuit F_8, single bridge short circuit F_9, double bridge short circuit F_{10}.

II. C. Valve short circuit protection principle

Valve short-circuit protection is used to detect valve short-circuit faults and inter-phase faults on the valve side of the converter transformer, to avoid overstressing the converter valve in case of a short-circuit and to protect the whole converter valve. The protection mainly collects three-phase currents (I_{VY}, I_{VD}) from the valve side Y winding and D winding of the converter transformer and DC pole bus current (I_{DCP}) and neutral current (I_{DCN}), calculates the difference between the valve side current of the converter transformer of the largest phase and the largest DC side current and compares it with the fixed value. Under normal operating conditions, the currents on both sides are balanced. When the difference between the AC side and DC side current is higher than the protection value, the protection will be activated, indicating that a short circuit occurs in the converter valve. The protection action criterion is:

$$I_{VY\_\max} - I_{D\_MAX} > I_{ref} \tag{13}$$

$$I_{VD\_\max} - I_{D\_MAX} > I_{ref} \tag{14}$$

$$I_{D\_\max} = MAX\left[I_{DCP}, I_{DCN}\right] \tag{15}$$

In the formula: I_{ref} of the Ⅰ section fixed value for 1.5p.u., no delay; Ⅱ section fixed value for 0.5p.u., delay 20ms; I_{DCP} indicates the current of the high-voltage side of the converter valve; I_{DCN} indicates the current of the low-voltage side of the converter valve; $I_{VY\_\max}$ denotes the maximum AC current on the valve side of the star-connected converter; $I_{VD\_\max}$ denotes the maximum AC current on the valve side of the angle-connected converter. $I_{D\_\max}$ denotes the maximum current on the DC side of the converter valve. The result of protection action is Ⅰ section rectifier side X blocking, tripping AC circuit breaker, inverter side S blocking, tripping AC circuit breaker. Section Ⅱ inverter side S blocking, tripping AC circuit breaker.

II. D. Discriminate valve state based on current timing characteristics

II. D. 1) Analysis for discriminating valve states based on current timing characteristics

Single-valve on/off transition conditions and current characteristics: When valve V_m has a trigger pulse P_m and is subjected to a positive valve voltage u_m, valve V_m, which is being shut down, begins to turn on and the valve current increases. When the valve current exceeds the prime current, the valve V_m remains in the on state until the conducting valve V_m is subjected to a reverse voltage. Thereafter, the valve current i_m begins to decrease until it reaches zero and meets the minimum arc extinguishing time, and the valve V_m completely shuts down and enters the off state.

According to the valve conduction and shutdown conditions, it is known that the valve end voltage should be introduced when judging the state of the valve. However, the actual engineering of the valve is not installed at the end of the voltage transformer, the end voltage can not be obtained directly. When the valve voltage is negative, the valve current only began to reduce, not for the valve current over the zero point moment. Therefore, even if the valve voltage is known, can not directly determine the moment of valve shutdown. Therefore, from the point of view of engineering practicality, this paper proposes that only from the characteristics of the current to construct the criteria for determining the valve state.

The switching discrimination between the on and off states, as well as the switching between the states of other valves, requires that the electrical quantity of the current moment and the state of the previous moment be determined jointly. The change rule of this electrical quantity and state quantity in the time series is referred to as the time series characteristic. Based on the timing characteristics of the current, it is determined whether a valve that is on will be turned off and whether a valve that is off will be turned on.

II. D. 2) Valve state discrimination based on current timing characteristics

According to the amplitude characteristics and timing characteristics of the three-phase AC current, the valve state can be determined. If the valve is off at the previous moment, when the valve pulse is triggered, the amplitude characteristics of the AC current and the positive and negative direction of the mutation are used to judge the on state of the anode valve and the cathode valve; if the valve is on at the previous moment, the valve is judged to be off when the AC current is less than the maintenance current and there is no mutation in the current.

Anode valve and cathode valve conduction state of the criterion is:

$$\begin{cases} |i_k| > I_{set1} \ \& \ \dfrac{i_k(t) - i_k(t-\Delta t)}{\Delta t} > K_{set1} \\ |i_k| > I_{set1} \ \& \ \dfrac{i_k(t-\Delta t) - i_k(t)}{\Delta t} > K_{set1} \end{cases} \tag{16}$$

where i_k is the valve-side AC current, $k = a, b, c$; $|i_k|$ is the absolute value of the valve-side AC current; Δt is a sampling interval, the actual engineering generally take 0.1ms; The I_{set1} is the threshold fixed value of the on-state, which is taken to be greater than the sum of the Prime and Leakage currents; K_{set1} is the threshold value of the rate of change of the AC current in the on state, which depends on the steepness of the change of the commutation current, and is related to the strength of the AC system support and the commutation angle.

The criterion for the valve off state is:

$$|i_k| < I_{set2} \ \& \left| \frac{i_k(t) - i_k(t-\Delta t)}{\Delta t} \right| < K_{set2} \tag{17}$$

In the formula, I_{set2} is the threshold value of the shutdown state, which is determined by the maintenance current of the valve; K_{set2} is the threshold value of the rate of change of the AC current in the shutdown state, which is the same as the value of K_{set1}.

II. D. 3) Correction of the valve on state

The failure of the converter to change phases tends to form a bypass loop operation state, which in turn diffuses into a single-phase bypass pair, where DC current flows along the bypass phase and all three-phase AC currents are zero. Both valves of the bypass pair are on, and the use of Eq. (17) will misjudge the two valves as off. In order to realize the correct calculation of valve currents, it is urgent to correct the valve on-state of the bypass pair.

The formation of a single-phase bypass pair is due to the fact that the two valves in the phase where the latest triggered valve is located are on throughout. Therefore, it is possible to correct the valve on-state of a single-phase bypass pair by utilizing the timing characteristics between the triggering pulses.

The criterion for constructing the single-phase bypass pair discrimination is:

$$\begin{cases} \max\left(i_{dH}, i_{dN}\right) - \max\left(|i_a|, |i_b|, |i_c|\right) > I_{set3} \\ \max\left(|i_a|, |i_b|, |i_c|\right) < I_{set4} \end{cases} \tag{18}$$

where I_{set3} is the phase change failure threshold fixed value, $I_{set3} = \max\left(k_1 i_{d\max}, I_0\right)$, k_1 is the ratio braking coefficient, $i_{d\max}$ is the DC side current max, I_0 is the starting current; I_{set4} is the threshold fixed value of the single-phase bypass pair, which is determined by the maintenance current of the valve.

The trigger pulse signal of the converter valve is latched and updated in real time. When the AC and DC current characteristics satisfy Eq. (18) for the first time, the number of the latched trigger pulse is extracted, and the phase where this valve is located can be determined as the bypass phase. Correct the valve in the bypass phase to be on, and the valves in the other phases to be off.

III. Experiment on fault diagnosis of converter valve based on modal analysis and multi-source data fusion

III. A. Validation of the effectiveness of discriminating valve states based on current timing features

III. A. 1) Fault discrimination based on voltage characteristics

For the three fault types, when they operate in the two states of commutator input and removal, the energy storage capacitors have different operating states, and the final output voltages of the commutator are different. No matter which type of short-circuit fault, voltage fluctuation will be generated, so as to produce a large circulating current between the upper and lower bridge arms. After the occurrence of a short-circuit fault, the amount of voltage change

of the storage capacitor element in the converter valve topology is not obvious, while the circulating current fault signal is relatively easy to detect, and the circulating current fault signal is generally also commonly used as a means of control in the precise location of faults in the control strategy.

Using MATLAB to build a five-level converter valve simulation model, the output voltage is five-level needs four half-bridge converter valve cascade, because the three-phase circuit is symmetrical, choose a phase as an example, to study the switching device IGBT short-circuit faults, the converter valve system, the a-phase output voltage and the fault of the converter valve on the bridge arm of the change in current. After the commutator valve short-circuit fault occurs, there are three abnormal working states of the energy storage capacitor, namely charging, bypassing and discharging. After the short-circuit of switching devices T_1 and T_2 occurs, the difference in the working state is that there is a discharging process of the energy storage capacitor after the short-circuit of T_2, and there is only a charging process in the case of the short-circuit of T_1, so that there is an increase in the voltage in the circuit in the case of a phase after the short-circuit of T_2. The voltage and current waveforms of the switching device IGBTs on different bridge arms after a short-circuit fault are shown in Fig. 2 (a~b), respectively.

Sequentially set the switch devices T_1, T_2 in Converter Valve 1 of the upper bridge arm, and T_1 in Converter Valve 2, and a short-circuit fault occurs in switch device T_1 of Converter Valve 1 in the lower bridge arm. The simulation results indicate that after the short circuit of switch device T_1 at the same position on Converter Valves 1 and 2 of the upper bridge arm, the output voltage waveforms of phase A nearly overlap. In other words, a short-circuit fault occurs at the same position of the IGBT in different converters on the same bridge arm, and its output voltage waveform is nearly identical to the bridge arm current. Observe waveforms 1 and 4 in the figure, set the short-circuit fault at the same position on different bridge arms, the output voltage and bridge arm current waveforms are very different, similarly, observe waveforms 2 and 4 set the fault at different positions on different bridge arms, the output voltage, bridge arm current waveforms are more different. That is, setting faults on different bridge arms will end up with significantly different output voltages and bridge arm currents.

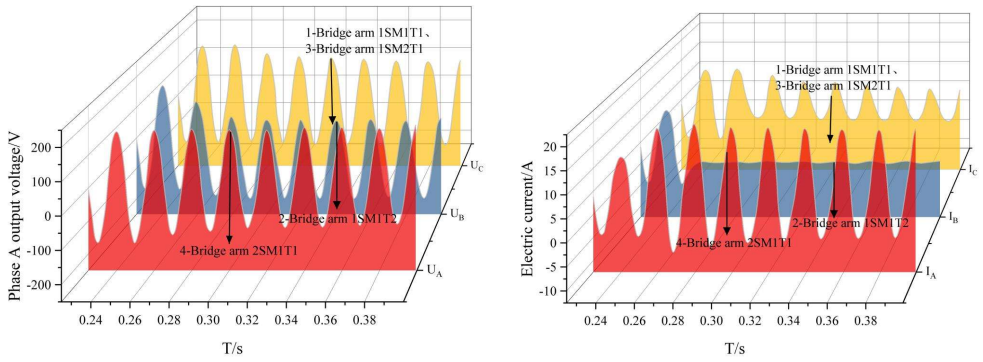

(a)Voltage (b)Electric current

Figure 2: Voltage and current after upper and lower arm failure

After a short-circuit fault occurs in the upper bridge arm converter valve 1 in the five-level topology, the capacitor voltage output waveform is shown in Figure 3. The abnormal charging and discharging of the energy storage capacitor makes the capacitance voltage have an obvious rising trend, and for the fault module localization detection, the bridge arm capacitance voltages are all obviously elevated, so the amount of voltage rise used is not suitable for the precise localization of the faulty converter valve.

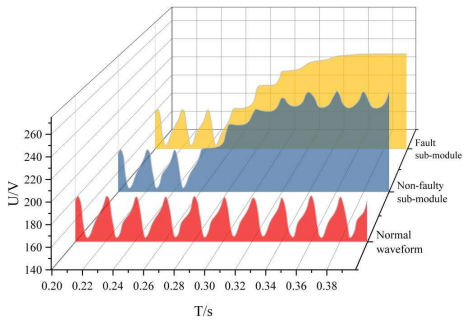

Figure 3: Submodule capacitance voltage waveform

III. A. 2) Fault discrimination based on timing characteristics

Converter valve in the IGBT high-frequency conduction and shutdown, resulting in a step voltage, and the step voltage changes very quickly, and even instantaneously complete the voltage mutation. Therefore, the circuit will produce a very large du/dt or di/dt, voltage in the process of sudden change, there will be a broadband signal, the broadband signal is equivalent to the time-varying source of the current-carrying conductor, multi-frequency signals will become a radiation antenna feeder, the number of converter valves to the outside world constantly radiating electromagnetic fields. When the short-circuit fault occurs in the IGBT in the converter valve, the energy storage capacitor will appear abnormal charging and discharging state, the normal operation and fault converter valve output voltage time domain waveform shown in Figure 4, which demonstrates the voltage change of the two ends of the capacitor. Switching devices in the converter valve short-circuit failure, capacitance of the abnormal discharge to form a large current, the impact of the circuit in the electronic devices, therefore, in the IGBT short-circuit converter valve will also produce a large internal voltage impact, and the IGBT together to form a radiated electromagnetic field, through the converter valve internal conductor to the outside of the electromagnetic wave, as an antenna structure, through the current, the voltage of the sudden change, resulting in a change in the surrounding magnetic field. The radiated electromagnetic field energy propagates outward in the medium.

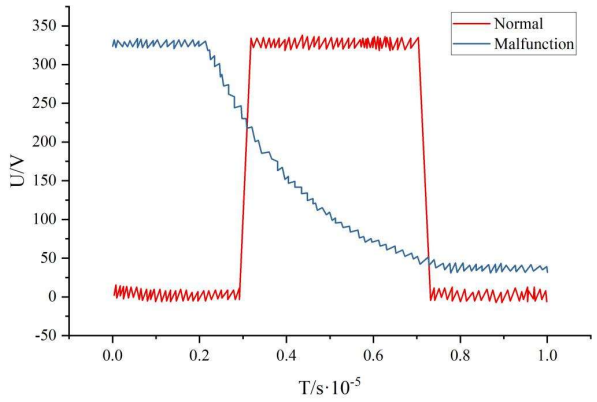

Figure 4: Comparison of output voltage time-domain waveforms

III. B. Engineering experimental validation

Calculating accurate valve current is the core key technology to solve the on-line detection of converter operation status. In order to calculate the current of each valve, it is necessary to determine the state of the converter valve. In order to verify the practicality of the proposed method to determine the valve state, this paper is based on the real-time recorded waveform data of the A-phase upper bridge arm of the North Channel Unit 1 of a megawatt-scale commissioned flexible DC project, including the capacitance capacity estimation of all the 405 power modules of one bridge arm. The data used for the calculations include:

(1) Sampled values of bridge arm currents for control received by the valve control with a period of 100 μs.

(2) Module trigger state and module capacitance voltage values received by the valve control from the power modules with a period of 50 μs.

The main sources of error in the capacitance estimation based on this project are as follows:

(1) Errors and noise in the bridge arm current sampling (current sensors and corresponding sampling and processing circuits);

(2) Error and noise of capacitive voltage sampling (high-precision voltage division sampling circuit);

(3) Bridge arm current, power module trigger state, module capacitor voltage value of the synchronization error. Among them, the bridge arm current has a weekly sampling delay of about 100μs, which is compensated in advance in the calculation. The synchronization error cannot be compensated and will affect the final result.

The calculation results are shown in Fig. 5, where each point corresponds to a power module, and its horizontal coordinate is the capacitance capacity record of the factory test, and the vertical coordinate is the capacitance capacity estimation based on the field data. Considering all 405 power modules of the whole bridge arm, the average value of the capacitance capacity of the factory test is 8.094mF, and the average value of the capacitance capacity estimated based on the field data is 8.096mF, with a relative error of 0.02%. This indicates that the estimation of capacitance capacity is basically unbiased.

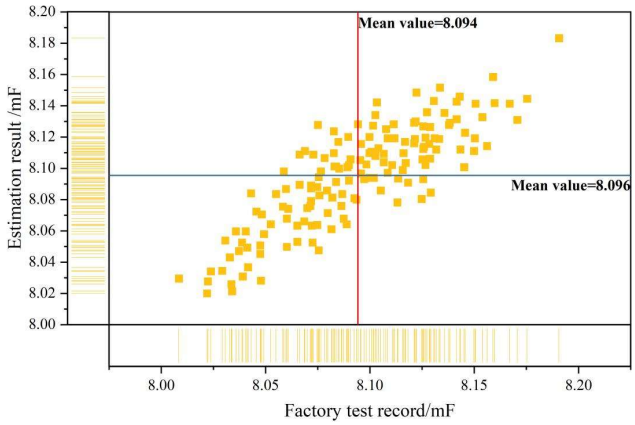

Figure 5: Comparison of the estimated capacitance results with the factory test results

The capacitance capacity estimated based on the field data is subtracted from the factory test data to obtain the error of capacitance capacity estimation (because the capacitance meter of the factory test is more accurate), and the distribution of the error is shown in Fig. 6. From the figure, it can be seen that the error of capacitance capacity estimation based on field data is within 1%. Considering the typical 2%~5% of capacitance capacity degradation as a sign of capacitance life, the method proposed in this paper is able to effectively differentiate the differences of each individual capacitor used in the project, and is able to satisfy the requirements of capacitance health status monitoring.

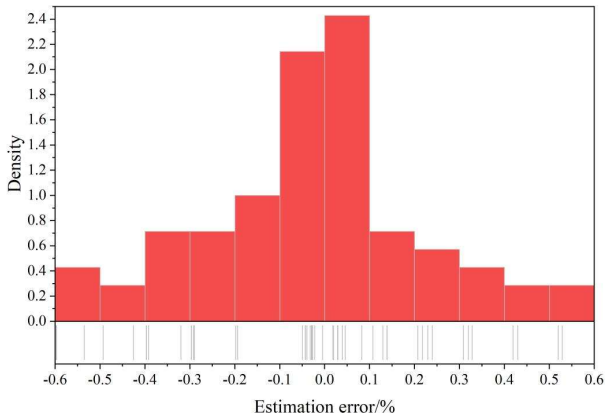

Figure 6: Distribution of capacitance estimation errors

In order to further verify the accuracy of the proposed method, 500 groups of tests are conducted for each of the short-circuit on the AC side of the converter valve, short-circuit on the converter valve, and short-circuit on the DC side of the converter valve, and the specific test results are shown in Table 1. The accuracy of fault detection reaches 99.88%, 99.86% and 99.91% respectively, which is close to 100%, indicating that the proposed method has high accuracy and can realize real-time monitoring of typical faults during the whole life cycle of the converter valve.

Table 1: Test Statistics Results

Fault type	Test group	Correct rate/%	Error rate/%
Short circuit on AC side of converter valve	500	99.88	0.12
Converter valve short circuit	500	99.86	0.14
Short circuit on DC side of converter valve	500	99.91	0.09

IV. Conclusion

Based on modal analysis and multi-source data fusion, this paper designs a method for extracting the time-varying laws of electrical features and state discrimination of the converter valve, and explores the application effect of the program through simulation experiments and engineering experiments.

Simulation experiments show that the use of voltage rise is not suitable for accurate location of faulty converter valves, and the use of time-domain features can effectively determine the state of converter valves. Considering all 405 power modules of the whole bridge arm, the average value of the capacitance capacity of the factory test is 8.094mF, and the average value of the capacitance capacity estimated based on the field data is 8.096mF, with a relative error of 0.02%. The error of capacitance capacity estimation based on field data is within 1%, which proves that the method proposed in this paper can effectively distinguish the differences of individual capacitance used in engineering. The detection accuracy of short circuit on AC side of converter valve, short circuit on converter valve and short circuit on DC side of converter valve reaches 99.88%, 99.86% and 99.91% respectively, which is close to 100%, indicating that the proposed method has high accuracy and can realize real-time monitoring of typical faults during the whole life cycle of converter valve.

Funding

This work was supported by the Science and Technology Project of China Southern Power Grid Company Limited under (CGYKJXM20220335).

References

[1] Qi, L., Shuai, Q., Cui, X., Fang, C., Sun, H., Wei, X., & Gao, C. (2016). Parameter Extraction and Wideband Modeling of ±1100 kV Converter Valve. IEEE Transactions on Power Delivery, 32(3), 1303-1313.

[2] Ji, Y., Yuan, Q., Zhou, C., Yang, M., Huang, X., Ma, L., & Zhao, H. (2025). Analysis of the Impact of Short Circuit Faults in Converter Valve Submodules on Valve Power Transmission. Energies, 18(6), 1496.

[3] Guo, J., Liu, H., Feng, L., & Zu, L. (2024). A fault diagnosis method for flexible converter valve equipment based on DSC-BIGRU-MA. Frontiers in Energy Research, 12, 1369360.

[4] Peng, B., Liu, X., Sun, H., Ding, J., Liu, K., Wang, J., ... & Qin, L. (2023). A novel prediction method for outlet water temperature of converter valve based on F-BP network. Energy Reports, 9, 879-887.

[5] Tarakesh, K. M. M., Chudamani, C., Dinesh, D., & Priyanka, B. (2022). Review On High Voltage Direct Current (Hvdc) Transmission System. Journal of Pharmaceutical Negative Results, 13.

[6] Bang, S., Kim, H. S., Koo, J. H., & Lee, B. W. (2021). Consideration of the insulation design method on a±200 kV converter valve unit in an HVDC converter hall. Energies, 14(8), 2296.

[7] Ding, C., Liu, Y., Zhu, P., Li, J., & Pu, G. (2023). Analysis of the Seismic Performance of±500 kV Flexible DC Converter Valves. Energies, 16(17), 6335.

[8] Kunpeng, Z., Junzheng, C., Wenmin, O., Baokui, S., Chong, G., & Hongzhou, L. (2017, February). Design of 6250A/±800kV UHVDC converter valve. In 13th IET International Conference on AC and DC Power Transmission (ACDC 2017) (pp. 1-6). IET.

[9] Yue, K., Pang, L., You, H., Li, S., Kong, D., Li, Y., ... & Liu, L. (2017). Reverse recovery characteristics of high power thyristors in HVDC converter valve. IEEE Transactions on Dielectrics and Electrical Insulation, 24(4), 2132-2140.

[10] Yin, S., Li, X., Li, J., Liu, D., & Cai, Z. (2021). Real-time virtual measurement technique for the thyristor valve current based on the converter terminal current. IEEE Transactions on Power Delivery, 37(5), 3447-3457.

[11] Liang, N., Tian, J., Liu, C., Gou, Y., Zhuo, F., & Wang, F. (2019, April). Research on Reliability Assessment of Thyristor in HVDC Converter Valve. In Journal of Physics: Conference Series (Vol. 1187, No. 2, p. 022016). IOP Publishing.

[12] Caiwang, S. H. E. N. G., Juanjuan, Z. H. A. N. G., Jie, L. I. U., Tingting, L. I., Jun, Y. A. N. G., & Libo, S. U. N. (2022). Thyristor Turn-off Time Under Actual Operational Condition in UHVDC Project Converter Valve. Power System Technology, 46(8), 3076-3083.

[13] Jianjian, G. A. O., Zhuokun, L. I. U., Guoqiang, L. I., Kai, Z. H. O. U., Ruicheng, D. A. I., Bi, Z. H. A. O., ... & Jianrui, S. O. N. G. (2024). A Review of Flexible DC Converter Valves and Valve Base Controller in China. Power System Technology, 48(9), 3890-3902.

[14] Wang, X., Li, J., Lu, Y., Yang, Y., Li, L., & Wang, W. (2024, August). Engineering Application of Valve Monitoring System for Flexible HVDC. In 2024 International Conference on HVDC (HVDC) (pp. 985-990). IEEE.

[15] Dai, J., Tan, F., Jiang, Y., Liang, Y., Lin, K., & Tong, K. (2025). Infrared image monitoring algorithm for converter valve equipment. AIP Advances, 15(3).

[16] Wang, Z., Xu, L., & Feng, A. (2025). Random forest algorithm and multi-source data fusion based on the converter valve electrical characteristics of time-varying law extraction method and condition monitoring technology research. J. COMBIN. MATH. COMBIN. COMPUT, 127, 7627-7644.